ENVIRONMENTAL RESEARCH
LETTERS

LETTER • OPEN ACCESS

# Siberian 2020 heatwave increased spring $CO_2$ uptake but not annual $CO_2$ uptake

To cite this article: Min Jung Kwon *et al* 2021 *Environ. Res. Lett.* **16** 124030

ENVIRONMENTAL RESEARCH
LETTERS

OPEN ACCESS

RECEIVED
27 July 2021

REVISED
29 October 2021

ACCEPTED FOR PUBLICATION
2 November 2021

PUBLISHED
25 November 2021



LETTER

# Siberian 2020 heatwave increased spring $CO_2$ uptake but not annual $CO_2$ uptake

**Min Jung Kwon[1], Ashley Ballantyne[1,2], Philippe Ciais[1], Ana Bastos[3], Frédéric Chevallier[1], Zhihua Liu[2], Julia K Green[1,5], Chunjing Qiu[1,4] and John S Kimball[2]**

[1] Laboratoire des Sciences du Climat et de l'Environnement, CEA-CNRS-UVSQ, Gif-sur-Yvette, France
[2] Department of Ecosystem and Conservation Science, University of Montana, Missoula, MT, United States of America
[3] Department Biogeochemical Integration, Max Planck Institute for Biogeochemistry, Jena, Germany
[4] UMR MIA 518, Université Paris-Saclay, INRAE, AgroParisTech, Paris, France
[5] Department of Environmental Science, Policy and Management, University of California at Berkeley, Berkeley, CA, United States of America

**E-mail:** minjung.kwon86@gmail.com

**Keywords:** high latitudes, extreme temperatures, $CO_2$ flux, seasonal transitions

Supplementary material for this article is available online

## Abstract

Siberia experienced an unprecedented strong and persistent heatwave in winter to spring of 2020. Using bottom–up and top–down approaches, we evaluated seasonal and annual $CO_2$ fluxes of 2020 in the northern hemisphere (north of 30 °N), focusing on Siberia where the pronounced heatwave occurred. We found that, over Siberia, $CO_2$ respiration loss in response to the pronounced positive winter temperature anomaly was greater than in previous years. However, continued warming in the spring enhanced photosynthetic $CO_2$ uptake, resulting in the largest seasonal transition in net ecosystem $CO_2$ exchange; that is, the largest magnitude of the switch from the net $CO_2$ loss in winter to net $CO_2$ uptake in spring until June. However, this exceptional transition was followed by the largest reduction in $CO_2$ uptake in late summer due to multiple environmental constraints, including a soil moisture deficit. Despite a substantial increase of $CO_2$ uptake by $22 \pm 9$ gC $m^{-2}$ in the spring in response to the heatwave, the mean annual $CO_2$ uptake over Siberia was slightly lower ($3 \pm 13$ gC $m^{-2}$ $yr^{-1}$) than the average of the previous five years. These results highlight the highly dynamic response of seasonal carbon fluxes to extreme temperature anomalies at high latitudes, indicating a seasonal compensation between abnormal uptake and release of $CO_2$ in response to extreme warmth that may limit carbon sink capacity in high northern latitudes.

## 1. Introduction

Global surface air temperature has increased rapidly since the beginning of the 20th century (0.08 °C per decade; Hartmann *et al* (2013)), but almost twice as fast in the Arctic (Serreze *et al* 2009, Cohen *et al* 2014). Extremely warm and persistent temperature anomalies have also increased significantly (Barriopedro *et al* 2011, Perkins-Kirkpatrick and Lewis 2020). By the end of this century, temperatures are predicted to increase by up to 11.4 °C in the Arctic (Collins *et al* 2013), in addition to more frequent and intense temperature extreme events.

Warming influences net $CO_2$ fluxes by altering the balance between photosynthesis and respiration throughout the year, and the magnitude of this response differs by season due to associated shifts in the prevailing limiting factors. In northern high latitudes, temperature is one of the dominant limiting factors of $CO_2$ uptake in spring. Seasonal thawing and the arrival of persistent warm temperatures in spring trigger leaf bud burst and flowering (Arft *et al* 1999, Aerts *et al* 2006, Ernakovich *et al* 2014), and can induce early onset of photosynthesis (gross primary production; GPP) and net $CO_2$ uptake (negative values of net ecosystem $CO_2$ exchange; NEE) by terrestrial ecosystems (Piao *et al* 2008, 2020, Park *et al* 2016, Li *et al* 2018, Parazoo *et al* 2018, Liu *et al* 2020). Yet an early onset of the growing season increases the chance of frost damage and a reduction in photosynthesis (Richardson *et al* 2018, Treharne *et al* 2019). In fall, ecosystem respiration ($R_{eco}$) is more responsive to warming than GPP (Piao *et al* 2008), which can be attributed to constraints on photosynthesis such as photoperiod, moisture, nutrient availability, and genetic or physiological controls linked to sink

limitations in plants (Arft *et al* 1999, Aerts *et al* 2006, Ernakovich *et al* 2014, Liu *et al* 2020, Zani *et al* 2020, Zhang *et al* 2020). In contrast, soil and root respiration continue in thawed soil (Blume-Werry *et al* 2016, Hicks Pries *et al* 2016). When the intensity of warming is high, as in the case of heatwaves, warming can either substantially increase $CO_2$ uptake in the absence of water stress (Wolf *et al* 2016, Bastos *et al* 2020a) or decrease it if soils become too dry (Ciais *et al* 2005, Reichstein *et al* 2013, Zscheischler *et al* 2014). The response to warming may also differ by ecosystem (Welp *et al* 2007, Bastos *et al* 2020a, Flach *et al* 2021) and species (Babst *et al* 2012, Niu *et al* 2014).

Siberia experienced an unprecedented heatwave in 2020 (Ciavarella *et al* 2021, Overland and Wang 2021): temperatures were 4.6 °C warmer than average from January to March (relative to 1981–2010) with extremely high temperatures persisting even longer in northern Siberia regions. Such sustained high temperature anomalies have probably not been observed in this area in the last 3 million years (Haywood *et al* 2020), but are expected to occur more frequently by the end of this century (Fan *et al* 2020). Although heatwaves often coincide with drought due to strong land-atmosphere coupling (Miralles *et al* 2019), the heatwave event over Siberia in 2020 did not coincide with drought, likely due to snow cover at the time of the heatwave and weak land-atmosphere coupling in high latitudes (Humphrey *et al* 2021). Here, we use the Siberian winter heatwave as an extreme event 'natural experiment' to evaluate its impact on the seasonal $CO_2$ balance at northern high latitudes. We compare NEE from several independent estimates over Siberia (>50 °N), and over Eurasia and North America (>30 °N; in the supplementary material). Specifically, we (a) quantify the changes in seasonal $CO_2$ fluxes of 2020 in response to the winter-to-spring warmth event, and (b) investigate whether changes in $CO_2$ fluxes during this early season influenced those in the later seasons, and the net annual $CO_2$ balance.

## 2. Methods

### 2.1. Seasonal variations and anomalies of climate and thaw date

We obtained climate data (ERA5 reanalysis)—air temperature, precipitation, and soil moisture—from 1979 through 2020 from the European Center for Medium-Range Weather Forecasts (ECMWF). We calculated the (linearly) detrended anomalies in climate variables for each grid cell relative to 1979–2019. We also used other climate variables as inputs for the simulation of a land surface model (LSM) and a multivariate Granger causality (MVGC) analysis. The spring thaw date of surface soil was calculated from the daily Freeze-Thaw Earth System Data Record v5.0 based on satellite microwave measurements (ESDR; Kim *et al* (2017, 2021)). The spring thaw date was defined annually as the earliest calendar day of the year when a forward-looking, 14-day running window contained at least 13 days when the land surface was classified as thawed, following Liu *et al* (2020). The ESDR data is available from www.ntsg.umt.edu/freeze-thaw/.

#### *2.1.1. Estimates of net ecosystem $CO_2$ exchange*

We compared NEE estimates from three independent approaches: an LSM with high-latitude processes (Organizing Carbon and Hydrology in Dynamic Ecosystems-aMeliorated Interactions between Carbon and Temperature; ORCHIDEE-MICT), a carbon flux model that integrates remote-sensing observations (Soil Moisture Active Passive—Level 4 Carbon; SMAP-L4C), and an atmospheric inversion system (Copernicus Atmosphere Monitoring Service combined with the second Orbiting Carbon Observatory; CAMS-OCO2). All of these estimates use different input data and methods, and each has its own strengths and weaknesses for detecting flux patterns (Schimel *et al* 2015, Bastos *et al* 2020c). The advantage of comparing them is that they are largely independent of each other, which enables us to better quantify uncertainties in seasonal $CO_2$ fluxes in response to the northern hemisphere heatwave event in 2020.

### 2.2. ORCHIDEE-MICT land surface model simulations

LSMs simulate physical, hydrological, and biogeochemical processes based on deterministic equations, with parameters usually calibrated from site observations. Although they may over- or underestimate fluxes under extreme climate conditions if the model is not well constrained (Schewe *et al* 2019, Bastos *et al* 2020b), they capture the magnitude and variability of $CO_2$ fluxes quite well for non-extreme climate conditions. Furthermore, LSMs allow us to diagnose the underlying processes (e.g. $R_{eco}$, GPP, and fires) contributing to patterns of anomalous net $CO_2$ fluxes and their potential environmental drivers. We used ORCHIDEE-MICT, which includes high-latitude processes such as permafrost, soil temperature, and soil carbon interactions, and a detailed calibration against multiple datasets (Guimberteau *et al* 2018). This model estimates global $CO_2$ fluxes close to the averages of LSM ensembles (Kondo *et al* 2020).

The ORCHIDEE-MICT (v8.7.1) LSM simulates energy, hydrologic, and carbon cycles, including processes that influence $CO_2$ exchange between the land and atmosphere on a 30 min to daily time-step. ERA5 reanalysis data (air temperature, humidity, pressure, shortwave and longwave incoming radiation, wind vectors, and precipitation) were used for performing a model simulation from 1979 to 2020 at $1^\circ \times 1^\circ$ resolution, with a fixed land cover map for the year 2010 (HYDE3.2; Klein Goldewijk *et al* (2017)). Daily flux rates were aggregated into monthly fluxes.

The model was run for 150 years looping (randomly mixing) the years from 1979 to 1990 to reach

equilibrium. Then, a soil accumulating spin-up submodule was run for 10,000 years to approximate soil carbon stock equilibrium at the start of the simulation. The full model was run for another 150 years to reach the equilibrium of physical variables and carbon pools and, finally, a transient run was conducted from 1979 to the end of 2020 following the same protocol as in Bastos *et al* (2020a). The global annual atmospheric $CO_2$ concentration for the model transient run was prescribed from the Mauna Loa Observatory record (NOAA, Earth System Research Laboratories).

### 2.3. Satellite data-driven carbon flux estimates (SMAP-L4C)

Satellite data-driven models estimate $CO_2$ fluxes and are forced by observations, such as phenology and soil moisture, to constrain gross $CO_2$ fluxes. They produce $CO_2$ fluxes with quite good performance (Luus and Lin 2015, Jones *et al* 2017); however, they can miss some nonlinear soil feedback, such as permafrost carbon decomposition. We used the daily $CO_2$ flux record from the NASA SMAP L4C product (Jones *et al* 2017), which is calibrated against global tower $CO_2$ flux measurements (FLUXNET; https://fluxnet.org/) and shows favorable performance and accuracy in high-latitude regions (Liu *et al* 2020).

Daily $CO_2$ fluxes from L4C cover a shorter period (2015–2020) than the LSM because the SMAP data are only available from 2015. The L4C product is a satellite data-driven carbon flux model using SMAP assimilation enhanced (level 4) surface (0–5 cm depth) and root zone (0–1 m depth) soil moisture and temperature (Reichle *et al* 2017), and MODIS (MODerate resolution Imaging Spectroradiometer) vegetation observations as key drivers. Other L4C meteorological inputs include surface daily minimum air temperature, atmospheric vapor pressure deficit, and incoming solar radiation provided from global reanalysis data. SMAP-L4C provides global daily estimates of NEE and component $CO_2$ fluxes for GPP and heterotrophic respiration (Rh) since March 31, 2015. The L4C calculations are processed at 1 km resolution and posted to a 9 km resolution global grid format. Daily rates of GPP, Rh, and NEE were aggregated into monthly, gridded carbon fluxes at $0.25\,^{\circ} \times 0.25\,^{\circ}$ resolution. We calculated NPP by subtracting NEE from Rh. The SMAP-L4C data is available from the National Snow and Ice Data Center (https://nsidc.org/data/spl4cmdl).

### 2.4. CAMS atmospheric inversion based on satellite column-average $CO_2$ retrievals

Atmospheric inversion models use atmospheric $CO_2$ observations and transport models to estimate the source and sink magnitudes of the land and ocean. Because of the usage of actual $CO_2$ concentrations, $CO_2$ flux estimates from inversions aggregate emissions and absorptions from all processes between the Earth's surface and the atmosphere (fire, land use change, etc; fossil fuel emissions are usually prescribed in atmospheric inversions). We used inversions of the CAMS, which show similar estimates of the inversion ensemble means (Peylin *et al* 2013, Kondo *et al* 2020).

Sources and sinks of $CO_2$ fluxes are diagnosed using releases FT20r3 (called CAMS-OCO2 hereafter; 2015–2020) and, to a lesser extent here, v20r1 (called CAMS-surface hereafter; 1979–2019) of the CAMS global atmospheric inversion (Chevallier *et al* 2019). CAMS-OCO2 assimilated the column-average $CO_2$ dry air-mole fraction ($XCO_2$) retrieved from the OCO-2 radiance measurements. Version 10r of NASA's Atmospheric $CO_2$ Observations from Space OCO-2 retrievals was used. CAMS-OCO2 covers the period between September 2014 and December 2020. The advantage of this OCO-2-driven inversion compared to the CAMS-surface inversion, which assimilates measurements of surface air samples, is its closer to real-time update, enabled by the rapid delivery of $XCO_2$ retrievals. However, CAMS-surface covers a much longer period, from 1979 until June 2020, thereby allowing a broader climatic perspective. Both CAMS inversions also used a full set of prior estimates of the $CO_2$ surface fluxes (including a climatology of natural fluxes over land simulated by the ORCHIDEE model) and represent atmospheric transport with the general circulation model of the Laboratoire de Meteorologie Dynamique (LMDz), nudged towards ERA5 horizontal winds. The inversion itself relies on a variational formulation of Bayes theorem. For this study, we used monthly averages of the net land-atmosphere fluxes of $CO_2$ at $1.89\,^{\circ}$ latitude $\times$ $3.75\,^{\circ}$ longitude resolution for both inversions.

### 2.5. Flux anomalies and transitions between quarters

After linearly detrending the monthly time series of $CO_2$ fluxes, we calculated 2020 anomalies compared to the averages of 2015–2019 for each quarter. We also quantified the seasonal 'transitions' of these $CO_2$ fluxes, defined as flux differences between successive quarters of the calendar year. We hypothesized that a strong $CO_2$ uptake in the early growing season will reduce $CO_2$ uptake in the late growing season due to the depletion of resources, e.g. soil moisture or nitrogen, and would make the transition in $CO_2$ fluxes between consecutive seasons stronger than usual. In order to quantify the transitions, we calculated the seasonal sum of fluxes by quarter (gC $m^{-2}$ $quarter^{-1}$ over each region; Q1: January–March; Q2: April–June; Q3: July–September; Q4: October–December) and their first order differences between successive quarters, following Yue *et al* (2017), providing a time series of transitions denoted as e.g. $NEE_{Q2\text{-}Q1}$ for $NEE_{Q2}$–$NEE_{Q1}$. Because negative NEE indicates net $CO_2$ uptake by land, more negative values of $NEE_{Q2\text{-}Q1}$ represent a larger change between $NEE_{Q1}$

(usually positive due to net $CO_2$ emission in Q1) and $NEE_{Q2}$ (usually negative due to net $CO_2$ uptake in the spring-centered Q2 period); i.e. a large $CO_2$ emission in Q1 and/or a large $CO_2$ uptake in Q2. $NEE_{Q1\text{-}Q4[-1]}$ refers to the NEE transition between Q1 of the current and Q4 of the previous year. To quantify the relationships between seasonal NEE transitions during the growing season, we performed a regression analysis between $NEE_{Q2\text{-}Q1}$ and $NEE_{Q3\text{-}Q2}$ by pooling all years. If more negative $NEE_{Q2\text{-}Q1}$ (switch to a stronger $CO_2$ uptake from Q1 to Q2) is followed by less negative $NEE_{Q3\text{-}Q2}$ (switch to a weaker $CO_2$ uptake from Q2 to Q3) due to environmental constraint in the later growing season, this transitional relationship will be shown as a negative slope in the regression. We performed all analyses over Siberia (>50 N, 40–180E), and additionally over Eurasia (>30 °N, 25 °W–180 °E) and North America (>30 °N, 25–180 °W), the results of which are shown in the supplementary material.

### 2.6. Granger causality analysis

To infer the causal impact of monthly air temperature, precipitation, soil moisture, and snow (SWE; predictor variables X) on NEE (response variable Y), we performed a MVGC analysis (Granger 1980) for each pixel location within the study region using data from 1979 to 2020. MVGC is a statistical technique that utilizes vector autoregressive models to determine whether the history of X (from the current and previous N months) adds information useful for the prediction of Y (if so, X is said to Granger-cause Y). For each 1 ° × 1 ° grid cell, first both predictor and response variables were linearly detrended, deseasonalized, and then normalized by their local mean and standard deviation for 1979–2020. Then an MVGC toolbox was used to generate a vector autoregressive model predicting the normalized NEE anomalies (Barnett and Seth 2014). Only the ORCHIDEE-MICT simulation was used for this analysis because the shorter time periods for SMAP-L4C and CAMS-OCO2 were not sufficient for robust results using MVGC.

Using each pixel's model output, normalized NEE anomalies were predicted for the full time period using all predictor variables that were deemed significant at a $P$ value of 0.1 based on an F-test with a null-hypothesis of 0-Granger causality ($NEE_{predicted,all}$). Then, NEE anomalies were again predicted, this time with one predictor variable $X$ set to 0 ($NEE_{predicted,withoutX}$). The overall fraction of variability explained by each predictor variable could then be quantified using equation (1), a sample equation of the fraction of variability in NEE explained by $X$:

$$\frac{\mathrm{var}\left(NEE_{predicted,all}\right) - \mathrm{var}\left(NEE_{predicted,withoutX}\right)}{\mathrm{var}\left(NEE_{normalized}\right)}. \quad (1)$$

To generate the fraction of variability in NEE explained by each predictor variable X per quarter, equation (1) was again used, but only for time-steps from the time series that fell during the quarter of interest.

In order to understand whether a predictor variable $X$ had a positive or negative impact on NEE, the time series of NEE predicted with one predictor variable $X$ removed ($NEE_{predicted,withoutX}$) was subtracted from the time series of NEE estimated using all predictor variables ($NEE_{predicted,all}$). These time series were again separated by quarter, and then the average values of each of the seasonal time series were calculated. Should the resulting predictor coefficient be positive (negative), then it can be inferred that the predictor variable has a positive (negative) influence on NEE anomalies.

## 3. Results

### 3.1. Climate anomalies

Air temperature was extremely high throughout the year 2020 over Siberia (figures 1(a), (c), and S1(a) (available online at stacks.iop.org/ERL/16/124030/mmedia) for the years 2015–2020), with some spatial and temporal (seasonal) variation. The heatwave had its largest extent from eastern Europe to eastern Siberia in Q1, and persisted in Q2 with an epicenter in northern central Siberia. Then, it further continued in the north of the Arctic circle in Q3 and Q4 (figure 1(a)). From exposure to an average 3.1 °C warmer air temperature in Q1 compared to the years 1979–2019 (over land, detrended anomaly), soil thawed *ca.* 5 days earlier relative to 1979–2019 across Siberia, with central Siberia showing the largest anomaly since the start of the observation period in 1979 (figure 1(b)). The precipitation anomaly of 2020 was at or above average until May but turned to below average from June onwards (figure 1(d)), with large spatial variation (figures S1(b) and S2(a)). The resulting soil moisture anomaly was comparable to the previous years until May but lower from June until the end of the year (figure 1(e)), especially in central and eastern Siberia (figures S1(c) and S2(b)). Higher air temperature anomalies coincided with greater precipitation (figure S3(a)), as well as with slight increases in soil moisture during Q1, but with slight decreases in soil moisture during Q3 (figure S3(b)). Increases in soil moisture were correlated spatially with positive precipitation anomalies in Q2 and Q3 (figure S3(c)).

### 3.2. Seasonal NEE anomalies

With positive temperature anomalies in Q1 and Q2, higher $NEE_{Q1}$ (larger emission) and lower $NEE_{Q2}$ (stronger uptake) were observed in 2020 compared to those of the previous five years (figures 2, 3, S4 and S5). The larger $CO_2$ uptake and an earlier shift from source to sink in Q2 was attributed to a large

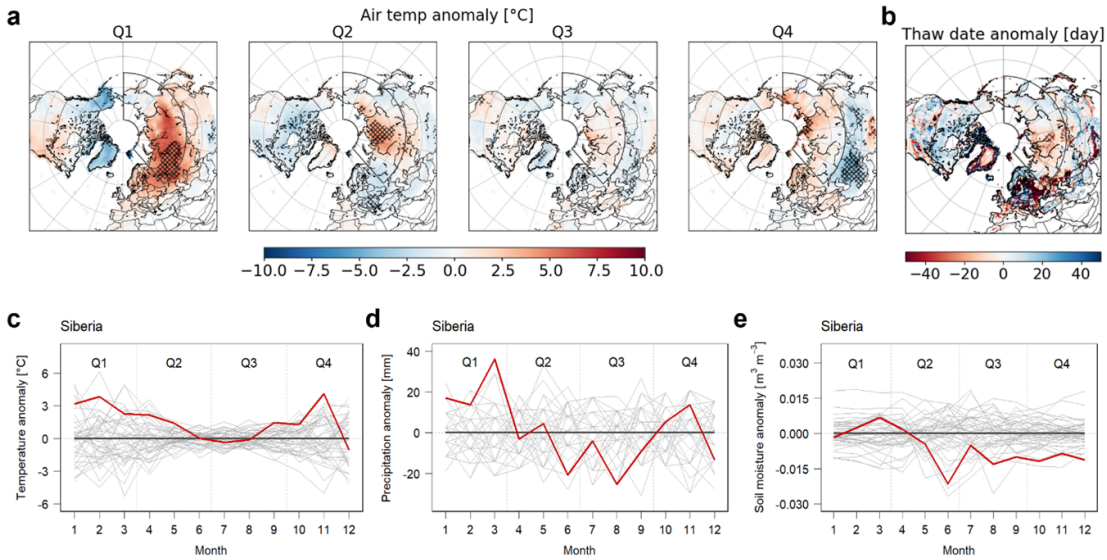


**Figure 1.** Detrended climate anomalies of 2020 relative to 1979–2019. Air temperature (ERA5 Reanalysis) anomalies in °C by quarter with positive values representing warmer than usual (a); and thaw date (ESDR freeze-thaw) anomalies (days) with negative value representing earlier soil thaw (b). Hatching denotes *z*-scores of 2020 greater than 2 for each pixel during 1979–2019, and black lines delineate the boundary of Siberian domain (a), (b). Monthly detrended anomalies of air temperature (ERA5 Reanalysis; (c)), precipitation (ERA5 Reanalysis; (d)), and soil moisture (ERA5 Reanalysis; (e)) over Siberia. Light gray lines represent individual years between 1979 and 2019 and the dark gray line is the average of these years (c)–(e). The red line is the 2020 anomaly.

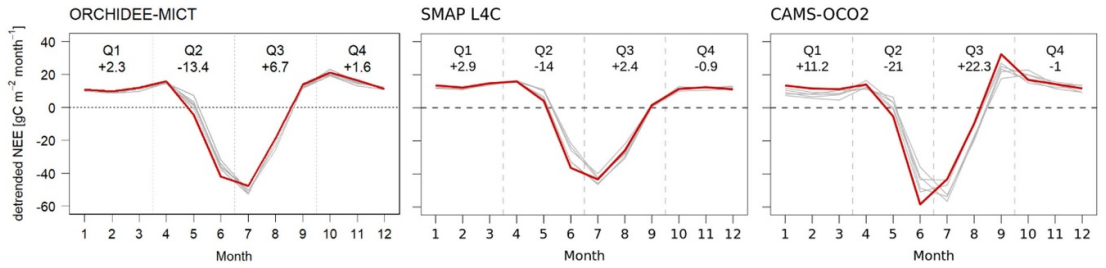


**Figure 2.** Linearly detrended NEE over Siberia estimated by ORCHIDEE-MICT, SMAP-L4C, and CAMS-OCO2. Light gray lines represent individual years between 2015 and 2019 and red lines represent 2020. Numbers represent the detrended anomalies relative to 2015–2019 for each quarter.

increase in $NPP_{Q2}$, despite increased $Rh_{Q2}$ in 2020 that partially offset the NEE changes (figures S5–S7). Less negative $NEE_{Q3}$ values and an earlier shift from net $CO_2$ uptake to net $CO_2$ emission were found in Q3 of 2020, and they were related to stronger decreases in $NPP_{Q3}$ than in previous years (figures S5–S7). The three estimates showed similar seasonal patterns until the peak of the growing season, with a transition from net $CO_2$ source to sink around May. However, SMAP-L4C showed a longer growing season with near-neutral $CO_2$ fluxes in September, while ORCHIDEE-MICT and CAMS-OCO2 indicated net $CO_2$ sources in the same month. In particular, CAMS-OCO2 showed large $CO_2$ emission peaks in September.

From the MVGC analysis based on 1979–2020, these seasonal NEE anomalies were explained largely by snow in Q1 and Q2 over Siberia (28.0% and 10.8% during Q1 and Q2, respectively), with more snow generally reducing $CO_2$ emissions or increasing $CO_2$ uptake, especially in the high latitudes (figure S8). Other predictor variables locally explained NEE anomalies; for instance, warmer air temperature enhanced $CO_2$ uptake in Q2 but $CO_2$ emission in Q3 over central Siberia (figure S8).

### 3.3. Seasonal transitions in NEE

The $NEE_{Q2\text{-}Q1}$ transition during 2020 was the most negative (switch to the strongest $CO_2$ uptake) of the recent record, with a difference of 15.7–32.3 gC $m^{-2}$ (32.7%–60.0%) compared to the average of 2015–2019 (table S1 and figures 3(a) and (b)). In contrast, the $NEE_{Q3\text{-}Q2}$ transition in 2020 was the most positive or the least negative (switch to the weakest $CO_2$ uptake), being 15.0–20.2 gC $m^{-2}$ (24.2%–306.2%) more positive than during any year since 2015 (table S1 and figures 3(a) and (b)). These enhanced and reduced uptake transitions were due to more $CO_2$ release (larger Rh) than average for $NEE_{Q1}$, more $CO_2$ uptake (larger NPP) than average for $NEE_{Q2}$, and less

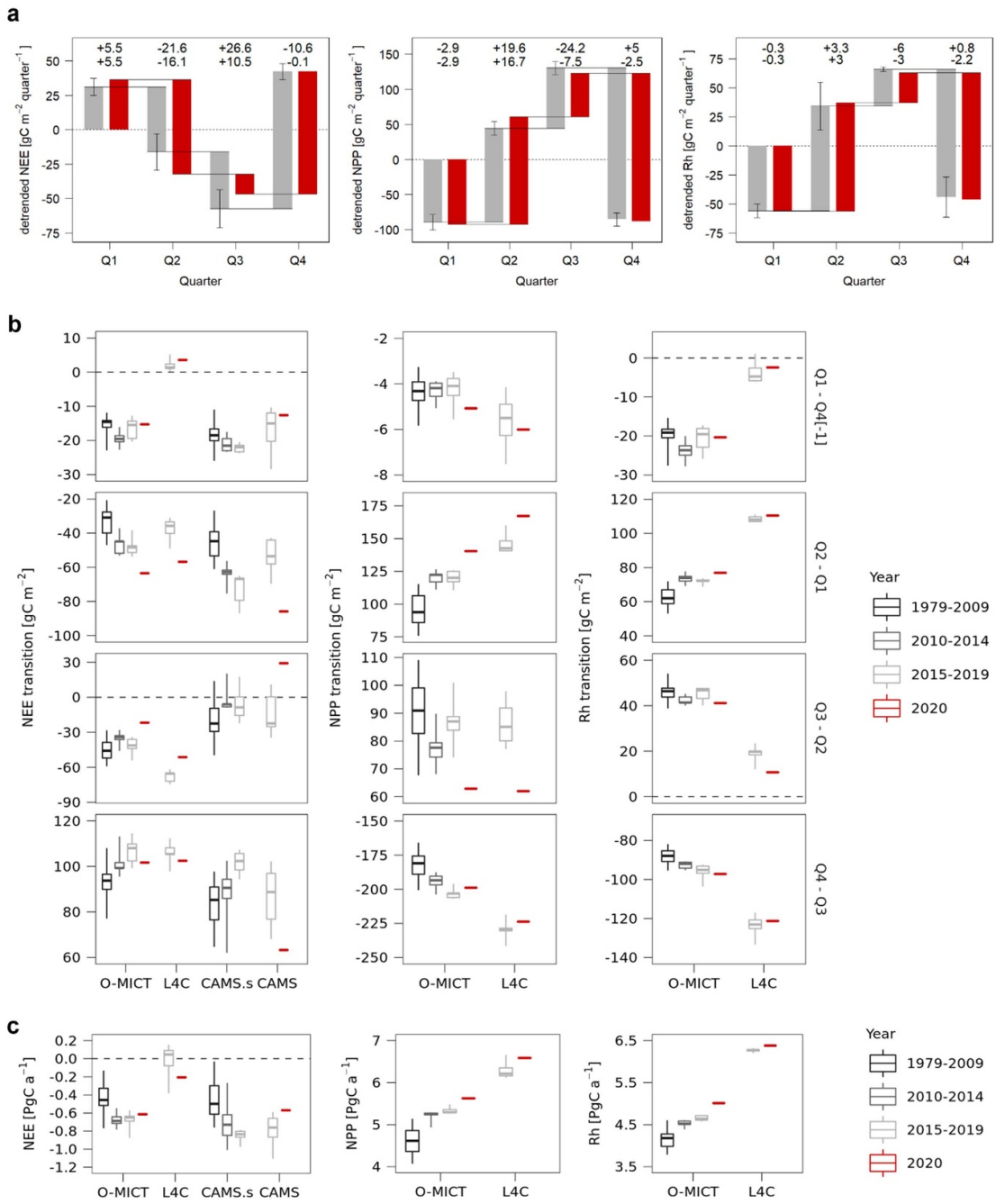


**Figure 3.** Cumulative detrended NEE, NPP, and Rh over Siberia in each quarter, in 2015–2019 (gray) and 2020 (red; (a)). Mean and standard deviation of years and estimates (O-MICT: ORCHIDEE-MICT, L4C: SMAP-L4C, and CAMS: CAMS-OCO2; O-MICT and SMAP-L4C in the case of NPP and Rh) are depicted for 2015–2019. The numbers represent the detrended anomalies of 2020 relative to 2015–2019 for each quarter (top) and cumulative sum (bottom). The height of each bar of (a) denotes the average of transitions in NEE, NPP, and Rh between quarters (b). Transitions are shown as boxplots showing 25%, 50%, and 75% quartiles, and minimum and maximum values for each year group. Annual sums of NEE, NPP, and Rh over Siberia of each year group are shown in the same manner (c).

$CO_2$ uptake than average for $NEE_{Q3}$ (figure 3(a)). This sequence of transition anomalies ($NEE_{Q2\text{-}Q1}$ then $NEE_{Q3\text{-}Q2}$) was largely driven by the abnormal increase in $NPP_{Q2\text{-}Q1}$ and decrease in $NPP_{Q3\text{-}Q2}$, despite concurrent changes in Rh, which partially offset the magnitudes of the large NPP swings (figure 3(b)). In summary, earlier and stronger onset of net $CO_2$ uptake (more negative $NEE_{Q2\text{-}Q1}$) was followed by an earlier decrease in the net $CO_2$ uptake and return to a $CO_2$ source in the late season (less negative $NEE_{Q3\text{-}Q2}$). This compensation in the transitions is clearly indicated by negative relationships between $NEE_{Q2\text{-}Q1}$ and $NEE_{Q3\text{-}Q2}$ not only in Siberia but in most regions north of 30 °N (figures 4 and S9), and from both NPP and Rh (figure S9).

### 3.4. Annual $CO_2$ balance

We found a higher $CO_2$ uptake in Q2 (more negative $NEE_{Q2}$) due to extensive warming, but it was followed by a subsequent decrease in $CO_2$ uptake or

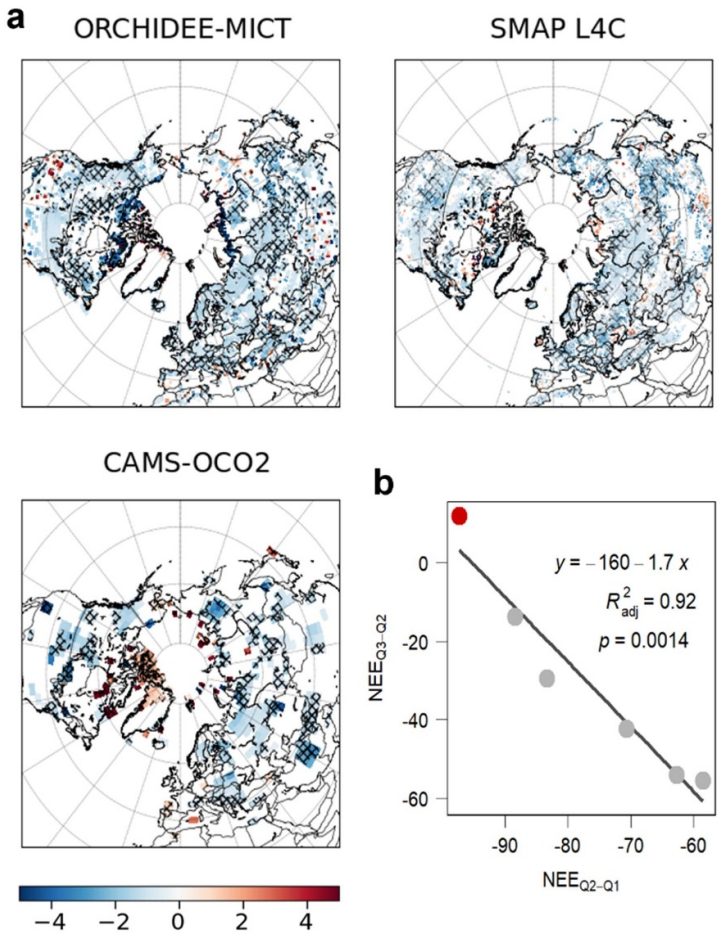


**Figure 4.** Regression slopes between the NEE transition from winter to spring ($NEE_{Q2-Q1}$) and the subsequent transition from spring to summer ($NEE_{Q3-Q2}$) for the period 2015–2020 estimated from ORCHIDEE-MICT, SMAP-L4C, and CAMS-OCO2 (a). Negative values of the relationship between $NEE_{Q2-Q1}$ and $NEE_{Q3-Q2}$ mean that a switch to more $CO_2$ uptake from winter to spring is systematically associated with a weaker intensification of the uptake from spring to summer. In other words, a 'good' spring for $CO_2$ uptake is auto-correlated with a 'bad' summer for $CO_2$ uptake. Positive values of the regression slopes are absent from nearly all estimates. Colors are shown for pixels that have $R^2 > 0.5$ and $P < 0.1$, and hatching represents $NEE_{Q3-Q2}$ of 2020 greater than the predicted value from the regression line. One example of the slope calculation from 55 °N 94 °E (ORCHIDEE-MICT; (b)). Each point represents each year from 2015 to 2020 and the red point is from 2020. When $R^2 > 0.5$ and $P < 0.1$ are met, the slope (e.g. −1.7) was shown on the map as color, and when the actual $NEE_{Q3-Q2}$ of 2020 was larger than the predicted value (red point above the predicted line), hatching was added.

increase in $CO_2$ release in Q3 (less negative $NEE_{Q3}$), offsetting the large spring $CO_2$ uptake. This strong seasonal compensation resulted in a slightly smaller annual sink by 0.1–0.2 PgC in 2020 (10.3%–28.4%) compared to the mean of 2015–2019 in ORCHIDEE-MICT and CAMS-OCO2 but a slightly larger annual sink by 0.2 PgC in SMAP-L4C compared to previous years (table S2 and figure 3(c)). In addition to the more negative $NEE_{Q2}$ and less negative $NEE_{Q3}$, more positive $NEE_{Q1}$ was consistently shown in the three estimates (figure 2) when the highest temperature anomalies were observed (figures 1(a) and (c)).

### 3.5. The year 2020 compared to previous decades

We also evaluated how the year 2020 behaved in the context of long-term trends based on the records of ORCHIDEE-MICT and CAMS-surface since 1979. Over the period of 1979–2019, ORCHIDEE-MICT and CAMS-surface long-term trends consistently showed more negative $NEE_{Q2-Q1}$ (switch to a larger spring $CO_2$ uptake) and less negative $NEE_{Q3-Q2}$ (switch to a smaller $CO_2$ uptake or a larger $CO_2$ release after the peak growing season) over time (figure 3(b)). The year 2020 showed general decreasing $NEE_{Q2-Q1}$ and increasing $NEE_{Q3-Q2}$ trends concurrent with the heatwave over Siberia (figure 3(b)); however, these strong transitions were abrupt considering the difference in seasonality between 2020 and 2010–2019 was as large as the decadal change from 1979–2009 to 2010–2019. Annually, Siberia showed larger $CO_2$ sinks from 2010 to 2014 compared to 1979–2009, and this increase was followed by a slight change in 2015–2019; i.e. a larger (CAMS-surface) or smaller (ORCHIDEE-MICT) $CO_2$ sink, followed by a slight reduction in net $CO_2$ uptake in 2020 (figure 3(c)), with continuous warming trends over time and the heatwave event in 2020 (figure S10).

## 4. Discussion

### 4.1. Heatwave effects on $CO_2$ seasonality and net annual carbon balance

The high northern latitude heatwave of 2020 was extremely widespread and persisted from winter to spring over Siberia, resulting in an earlier start of summer. Unlike the usual concurrence of heatwave and drought, the heatwave over Siberia in 2020 occurred in the presence of snow cover and higher than average precipitation until May. Although tight feedback processes among high temperature, dry soil, and increased vapor pressure deficit are often found in the mid-latitudes (Miralles *et al* 2019), this land-atmosphere coupling (feedback) tends to be weaker at high latitudes (Humphrey *et al* 2021). Abundant snowmelt water and precipitation maintained sufficient soil moisture until May; thus, strong $CO_2$ uptake was dominant in the absence of soil moisture deficits. This increased $CO_2$ uptake in response to the heatwave is different from the reduced $CO_2$ uptake that has been observed during other concurrent heatwave and drought events, e.g. in Europe (Ciais *et al* 2005, Zscheischler *et al* 2014, Bastos *et al* 2020a). Although specific plant functional types can alleviate the reduction in $CO_2$ uptake in response to heatwave and drought events (Flach *et al* 2018, 2021), strong $CO_2$ uptake over Siberia in 2020 emphasizes the role of sufficient soil moisture in sustaining photosynthesis. It is also supported by the MVGC analysis indicating negative influence of snow (SWE) on NEE anomalies; i.e. more snow results in relatively larger net $CO_2$ uptake in the early growing season. Soil moisture did little to explain the NEE anomalies, possibly due to mixed effects of increasing soil moisture during snowmelt and decreasing soil moisture during photosynthesis over multiple months.

The strong $CO_2$ uptake in early summer, however, could not persist over the whole growing season despite continuing positive temperature anomalies, possibly due to one or more environmental constraints: (a) increased photosynthesis and evapotranspiration activity coincided with a negative precipitation anomaly from June to September. Soil moisture was depleted more quickly because of the increased evapotranspiration demand, and was not replenished by precipitation during the growing season. The resulting increase in dry soil conditions reduced photosynthesis and $CO_2$ uptake later in the summer, as seen by Buermann *et al* (2018), Lian *et al* (2020), and Zhang *et al* (2020) in the mid-latitudes. (b) The depletion of nitrogen availability in the late growing season (Haddad *et al* 2002, van Wijk *et al* 2003, Reich and Hobbie 2013) and a reduction in plant access to soil nutrients (figure 1(e); Moyano *et al* (2013)) may have limited further $CO_2$ uptake in the late growing season. (c) Limited carbon sink capacity of plants, e.g. carbohydrate accumulation suppressing photosynthesis, could have contributed to earlier senescence following enhanced spring photosynthesis (Paul and Foyer 2001, Keenan and Richardson 2015, Zani *et al* 2020). All of these factors (or combinations of them) could have ceased further active $CO_2$ sequestration in the late summer over Siberia. In addition, active photosynthesis in the early growing season may have fueled $CO_2$ release in later seasons (Brooks *et al* 2004, Jeong *et al* 2018). The emerging relationship of greater NPP in Q2 and increased NEE (reduced $CO_2$ uptake or increased $CO_2$ emission) in Q3 and Q4 supports this explanation. Overall, early onset of net $CO_2$ uptake or strong net $CO_2$ uptake in the early growing season did not necessarily enhance the net annual $CO_2$ sink, and even led to a smaller $CO_2$ sink in 2020 when estimated by the inversion and the process-based model (figure 3(c)).

### 4.2. Discrepancies among estimates

While the extreme seasonal transitions of 2020 in comparison to previous years were consistent for each model estimate (interannual variations within each estimate), there were some discrepancies among model estimates. Annual sums of both NPP and Rh over Siberia in 2020 were the highest or second highest compared to those of 2015–2019, and ORCHIDEE-MICT simulated a smaller NEE sink than the mean of 2015–2019, whereas SMAP-L4C simulated a larger sink. This discrepancy can be attributed to the different underlying processes and varying sensitivity of NPP and Rh in response to the extreme climate condition. For example, SMAP-L4C showed a noticeable decrease in Rh in June 2020, which could be attributed to stronger sensitivity of respiration to soil moisture depletion. (a) The underrepresentation of SOC contributions to Rh from deeper soil layers (Endsley *et al* 2020, Yi *et al* 2020), which can underestimate respiration during fall when surface soils freeze and deeper soil layers remain thawed, and (b) near-neutral $CO_2$ balances of SMAP-L4C, which are associated with the relatively short operational record, may also contribute to the discrepancy. Differences in model inputs and underlying model algorithms and assumptions may have further contributed to differences in the timing and magnitudes of seasonal transitions between ORCHIDEE-MICT and SMAP-L4C.

One of the limitations for direct comparison between bottom–up estimates and inverse modeling is the $CO_2$ fluxes that they include. Biogenic NEE of inverse modeling includes all $CO_2$ fluxes in addition to photosynthesis and respiration, such as $CO_2$ emissions from wildfire, land use change, and lateral transport. The largest wildfire activities and $CO_2$ emission were observed in June–August 2020 in the Arctic Circle (CAMS 2021), and annually 173–205 TgC was emitted by fire over Siberia in 2020 when estimated by ORCHIDEE-MICT, Global Fire Assimilation System v1.2 and the Global Fire Emissions Database (GFED) v4.1 (figure S11; note that

GFED fire emissions for 2020 are preliminary). These fire emissions over Siberia were higher than the average of previous years. However, including fire $CO_2$ emissions does not change the interannual NEE patterns and anomalies of 2020 as shown in this study (figure S12). Adding fire $CO_2$ emissions did not bring the three estimates closer (figure S12), as other processes, such as land use change and lateral transport, are not included in bottom–up estimates, which can be sources of discrepancy between bottom–up estimates and inversions (e.g. Jung *et al* (2020), Kondo *et al* (2020)).

### 4.3. Implications for the long-term carbon balance at high latitudes

In this study, we found that extremely warm spring temperatures over Siberia in 2020 significantly enhanced spring $CO_2$ uptake by the land surface. However, although warmer than usual temperatures persisted until the end of the year, potential environmental constraints reduced $CO_2$ uptake in the summer, and Siberia ended up as a smaller annual $CO_2$ sink in 2020 than in previous, less warm years. Our results indicate that the responses of terrestrial ecosystems to extreme climate events can be both immediate (due to near-term responses to climate forcings) and lagged (due to accumulating environmental constraints), and that an enhancement in $CO_2$ uptake during an extended growing season will not necessarily lead to a large net annual $CO_2$ sink. The ecosystem carbon response can be lagged even by years, e.g. suppression of $CO_2$ uptake can occur in subsequent years through accelerated soil respiration (Arnone III *et al* 2008, Babst *et al* 2012) and increased insect outbreaks (Bjerke *et al* 2014), or fire $CO_2$ emission can increase after warm summers (Scholten *et al* 2021); thus, multi-year observations would be needed to fully quantify the heatwave impacts on important $CO_2$ cycle processes and their legacy effects on the high-latitude carbon budget.

Warming has increased land $CO_2$ uptake over the last five decades (Ciais *et al* 2019b, Piao *et al* 2020), and stronger thermal optimality of photosynthesis compared to respiration to warming implies that future warming in the Arctic may further enhance carbon uptake (Saxe *et al* 2001, Niu *et al* 2012). However, carbon uptake sensitivity to warming has decreased in the last few decades, especially in high latitudes (Piao *et al* 2017, Yin *et al* 2018, Bastos *et al* 2019). Our findings also show that the increasing carbon uptake rate paused in recent years, and the year 2020, which experienced a record warming, was a slightly smaller carbon sink in Siberia, as shown in the ORCHIDEE-MICT and CAMS-OCO2 results. The different magnitudes of acclimation of photosynthesis and respiration to warming may change this trend (Lombardozzi *et al* 2015, Reich *et al* 2016), and further observation and analysis would be needed to fully explain the relationship between net carbon uptake and warming. Nonetheless, our results imply that, despite the enhanced seasonal $CO_2$ uptake by land due to a heatwave with no concurrent drought, extremely warm temperatures do not necessarily result in significantly greater net annual carbon sink activity in the northern high latitudes due to compensating seasonal responses in ecosystem productivity and respiration. The timing and duration of heatwaves and other environmental constraints all play a role in the seasonal and annual carbon cycle. Considering substantial decreases in $CO_2$ uptake with concurrent drought (Ciais *et al* 2005, Zscheischler *et al* 2014) and slight decreases in the annual $CO_2$ uptake without drought, as shown in this study, more frequent and intense heatwave events in the high latitudes are likely to reduce land carbon uptake in the future.

## Data availability statement

The data that support the findings of this study are available upon reasonable request from the authors.

## Acknowledgments

This research was supported by the l'Agence Nationale de la Recherche (Make Our Planet Great Again; ANR-18-MPGA-0007).

## Conflict of interest

The authors declare no conflict of interest.

## ORCID iDs

Min Jung Kwon https://orcid.org/0000-0002-7330-2320
Philippe Ciais https://orcid.org/0000-0001-8560-4943
Ana Bastos https://orcid.org/0000-0002-7368-7806
Frédéric Chevallier https://orcid.org/0000-0002-4327-3813
Zhihua Liu https://orcid.org/0000-0002-0086-5659
Julia K Green https://orcid.org/0000-0002-8466-2313

## References

Aerts R, Cornelissen J H C and Dorrepaal E 2006 Plant performance in a warmer world: general responses of plants from cold, northern biomes and the importance of winter and spring events *Plant Ecol.* **182** 65–77

Arft A *et al* 1999 Responses of tundra plants to experimental warming: meta-analysis of the international tundra experiment *Ecol. Monogr.* **69** 491–511

Arnone III J A *et al* 2008 Prolonged suppression of ecosystem carbon dioxide uptake after an anomalously warm year *Nature* **455** 383–6

Babst F, Carrer M, Poulter B, Urbinati C, Neuwirth B and Frank D 2012 500 years of regional forest growth variability and links to climatic extreme events in Europe *Environ. Res. Lett.* **7** 045705

Barnett L and Seth A K 2014 The MVGC multivariate Granger causality toolbox: a new approach to Granger-causal inference *J. Neurosci. Methods* **223** 50–68

Barriopedro D, Fischer E M, Luterbacher J, Trigo R M and García-Herrera R 2011 The hot summer of 2010: redrawing the temperature record map of Europe *Science* **332** 220–4

Bastos A *et al* 2019 Contrasting effects of $CO_2$ fertilization, land-use change and warming on seasonal amplitude of Northern Hemisphere $CO_2$ exchange *Atmos. Chem. Phys.* **19** 12361–75

Bastos A *et al* 2020a Direct and seasonal legacy effects of the 2018 heat wave and drought on European ecosystem productivity *Sci. Adv.* **6** eaba2724

Bastos A *et al* 2020b Impacts of extreme summers on European ecosystems: a comparative analysis of 2003, 2010 and 2018 *Phil. Trans. R. Soc.* B **375** 20190507

Bastos A *et al* 2020c Sources of uncertainty in regional and global terrestrial $CO_2$ exchange estimates *Glob. Biogeochem. Cycles* **34** e2019GB006393

Bjerke J W, Karlsen S R, Høgda K A, Malnes E, Jepsen J U, Lovibond S, Vikhamar-Schuler D and Tømmervik H 2014 Record-low primary productivity and high plant damage in the Nordic Arctic Region in 2012 caused by multiple weather events and pest outbreaks *Environ. Res. Lett.* **9** 084006

Blume-Werry G, Wilson S D, Kreyling J and Milbau A 2016 The hidden season: growing season is 50% longer below than above ground along an arctic elevation gradient *New Phytol.* **209** 978–86

Brooks P D, McKnight D and Elder K 2004 Carbon limitation of soil respiration under winter snowpacks: potential feedbacks between growing season and winter carbon fluxes *Glob. Change Biol.* **11** 231–8

Buermann W *et al* 2018 Widespread seasonal compensation effects of spring warming on northern plant productivity *Nature* **562** 110–14

CAMS 2021 Copernicus reveals summer 2020's Arctic wildfires set new emission records (available at: https://atmosphere.copernicus.eu/copernicus-reveals-summer-2020s-arctic-wildfires-set-new-emission-records)

Chevallier F, Remaud M, O'Dell C W, Baker D, Peylin P and Cozic A 2019 Objective evaluation of surface- and satellite-driven carbon dioxide atmospheric inversions *Atmos. Chem. Phys.* **19** 14233–51

Ciais P *et al* 2005 Europe-wide reduction in primary productivity caused by the heat and drought in 2003 *Nature* **437** 529–33

Ciais P *et al* 2019b Five decades of northern land carbon uptake revealed by the interhemispheric $CO_2$ gradient *Nature* **568** 221–5

Ciavarella A *et al* 2021 Prolonged Siberian heat of 2020 almost impossible without human influence *Clim. Change* **166** 9

Cohen J *et al* 2014 Recent Arctic amplification and extreme mid-latitude weather *Nat. Geosci.* **7** 627–37

Collins M *et al* 2013 Long-term climate change: projections, commitments and irreversibility *Climate Change 2013: The Physical Science Basis. Contribution of Working Group I to the Fifth Assessment Report of the Intergovernmental Panel on Climate Change* ed T F Stocker, D Qin, G-K Plattner, M M B Tignor, S K Allen, J Boschung, A Nauels, Y Xia, V Bex and P M Midgley (Cambridge: Cambridge University Press) pp 1029–136

Endsley K A, Kimball J S, Reichle R H and Watts J D 2020 Satellite monitoring of global surface soil organic carbon dynamics using the SMAP level 4 carbon product *J. Geophys. Res.: Biogeosci.* **125** e2020JG006100

Ernakovich J G, Hopping K A, Berdanier A B, Simpson R T, Kachergis E J, Steltzer H and Wallenstein M D 2014 Predicted responses of arctic and alpine ecosystems to altered seasonality under climate change *Glob. Change Biol.* **20** 3256–69

Fan X, Duan Q, Shen C, Wu Y and Xing C 2020 Global surface air temperatures in CMIP6: historical performance and future changes *Environ. Res. Lett.* **15** 104056

Flach M, Brenning A, Gans F, Reichstein M, Sippel S and Mahecha M D 2021 Vegetation modulates the impact of climate extremes on gross primary production *Biogeosciences* **18** 39–53

Flach M, Sippel S, Gans F, Bastos A, Brenning A, Reichstein M and Mahecha M D 2018 Contrasting biosphere responses to hydrometeorological extremes: revisiting the 2010 western Russian heatwave *Biogeosciences* **15** 6067–85

Granger C W J 1980 Testing for causality: a personal viewpoint *J. Econ. Dyn. Control* **2** 329–52

Guimberteau M *et al* 2018 ORCHIDEE-MICT (v8.4.1), a land surface model for the high latitudes: model description and validation *Geosci. Model Dev.* **11** 121–63

Haddad N M, Tilman D and Knops J M H 2002 Long-term oscillations in grassland productivity induced by drought *Ecol. Lett.* **5** 110–20

Hartmann D L *et al* 2013 Observations: atmosphere and surface *Climate Change 2013: The Physical Science Basis. Contribution of Working Group I to the Fifth Assessment Report of the Intergovernmental Panel on Climate Change* (Cambridge: Cambridge University Press) 159–254

Haywood A M *et al* 2020 The pliocene model intercomparison project phase 2: large-scale climate features and climate sensitivity *Clim. Past* **16** 2095–123

Hicks Pries C E, Schuur E A G, Natali S M and Crummer K G 2016 Old soil carbon losses increase with ecosystem respiration in experimentally thawed tundra *Nat. Clim. Change* **6** 214–18

Humphrey V, Berg A, Ciais P, Gentine P, Jung M, Reichstein M, Seneviratne S I and Frankenberg C 2021 Soil moisture–atmosphere feedback dominates land carbon uptake variability *Nature* **592** 65–9

Jeong S-J *et al* 2018 Accelerating rates of Arctic carbon cycling revealed by long-term atmospheric CO2 measurements *Sci. Adv.* **4** eaao1167

Jones L A *et al* 2017 The SMAP level 4 carbon product for monitoring ecosystem land–atmosphere CO2 exchange *IEEE Trans. Geosci. Remote Sens.* **55** 6517–32

Jung M *et al* 2020 Scaling carbon fluxes from eddy covariance sites to globe: synthesis and evaluation of the FLUXCOM approach *Biogeosciences* **17** 1343–65

Keenan T F and Richardson A D 2015 The timing of autumn senescence is affected by the timing of spring phenology: implications for predictive models *Glob. Change Biol.* **21** 2634–41

Kim Y, Kimball J S, Glassy J and Du J 2017 An extended global Earth system data record on daily landscape freeze–thaw status determined from satellite passive microwave remote sensing *Earth Syst. Sci. Data* **9** 133–47

Kim Y, Kimball J S, Glassy J and Du J 2021 MEaSUREs global record of daily landscape freeze/thaw status, version 05 [1979–2020] *National Snow and Ice Data Center* (https://doi.org/10.5067/MEASURES/CRYOSPHERE/nsidc0477.004)

Klein Goldewijk K, Beusen A, Doelman J and Stehfest E 2017 Anthropogenic land use estimates for the Holocene—HYDE 3.2 *Earth Syst. Sci. Data* **9** 927–53

Kondo M *et al* 2020 State of the science in reconciling top-down and bottom-up approaches for terrestrial CO2 budget *Glob. Change Biol.* **26** 1068–84

Li Z *et al* 2018 Non-uniform seasonal warming regulates vegetation greening and atmospheric CO2 amplification over northern lands *Environ. Res. Lett.* **13** 124008

Lian X *et al* 2020 Summer soil drying exacerbated by earlier spring greening of northern vegetation *Sci. Adv.* **6** eaax0255

Liu Z *et al* 2020 Increased high-latitude photosynthetic carbon gain offset by respiration carbon loss during an anomalous warm winter to spring transition *Glob. Change Biol.* **26** 682–96

Lombardozzi D L, Bonan G B, Smith N G, Dukes J S and Fisher R A 2015 Temperature acclimation of photosynthesis and respiration: a key uncertainty in the carbon cycle-climate feedback *Geophys. Res. Lett.* **42** 8624–31
Luus K A and Lin J C 2015 The polar vegetation photosynthesis and respiration model: a parsimonious, satellite-data-driven model of high-latitude CO2 exchange *Geosci. Model Dev.* **8** 2655–74
Miralles D G, Gentine P, Seneviratne S I and Teuling A J 2019 Land-atmospheric feedbacks during droughts and heatwaves: state of the science and current challenges *Ann. New York Acad. Sci.* **1436** 19–35
Moyano F E, Manzoni S and Chenu C 2013 Responses of soil heterotrophic respiration to moisture availability: an exploration of processes and models *Soil Biol. Biochem.* **59** 72–85
Niu S *et al* 2012 Thermal optimality of net ecosystem exchange of carbon dioxide and underlying mechanisms *New Phytologist* **194** 775–83
Niu S, Luo Y, Li D, Cao S, Xia J, Li J and Smith M D 2014 Plant growth and mortality under climatic extremes: an overview *Environ. Exp. Bot.* **98** 13–19
Overland J E and Wang M 2021 The 2020 Siberian heat wave *Int. J. Climatol.* **41** E2341–6
Parazoo N C *et al* 2018 Spring photosynthetic onset and net CO2 uptake in Alaska triggered by landscape thawing *Glob. Change Biol.* **24** 3416–35
Park T, Ganguly S, Tømmervik H, Euskirchen E S, Høgda K A, Karlsen S R, Brovkin V, Nemani R R and Myneni R B 2016 Changes in growing season duration and productivity of northern vegetation inferred from long-term remote sensing data *Environ. Res. Lett.* **11** 084001
Paul M J and Foyer C H 2001 Sink regulation of photosynthesis *J. Exp. Bot.* **52** 1383–400
Perkins-Kirkpatrick S E and Lewis S C 2020 Increasing trends in regional heatwaves *Nat. Commun.* **11** 3357
Peylin P *et al* 2013 Global atmospheric carbon budget: results from an ensemble of atmospheric $CO_2$ inversions *Biogeosciences* **10** 6699–720
Piao S *et al* 2008 Net carbon dioxide losses of northern ecosystems in response to autumn warming *Nature* **451** 49–52
Piao S *et al* 2017 Weakening temperature control on the interannual variations of spring carbon uptake across northern lands *Nat. Clim. Change* **7** 359–63
Piao S *et al* 2020 Characteristics, drivers and feedbacks of global greening *Nat. Rev. Earth Environ.* **1** 14–27
Reich P B and Hobbie S E 2013 Decade-long soil nitrogen constraint on the CO2 fertilization of plant biomass *Nat. Clim. Change* **3** 278–82
Reich P B, Sendall K M, Stefanski A, Wei X, Rich R L and Montgomery R A 2016 Boreal and temperate trees show strong acclimation of respiration to warming *Nature* **531** 633–6
Reichle R H *et al* 2017 Global assessment of the SMAP Level-4 surface and root-zone soil moisture product using assimilation diagnostics *J. Hydrometeorol.* **18** 3217–37
Reichstein M *et al* 2013 Climate extremes and the carbon cycle *Nature* **500** 287–95
Richardson A D *et al* 2018 Ecosystem warming extends vegetation activity but heightens vulnerability to cold temperatures *Nature* **560** 368–71
Saxe H, Cannell M G R, Johnsen Ø, Ryan M G and Vourlitis G 2001 Tree and forest functioning in response to global warming *New Phytologist* **149** 369–99
Schewe J *et al* 2019 State-of-the-art global models underestimate impacts from climate extremes *Nat. Commun.* **10** 1005
Schimel D, Stephens B B and Fisher J B 2015 Effect of increasing CO2 on the terrestrial carbon cycle *PNAS* **112** 436–41
Scholten R C, Jandt R, Miller E A, Rogers B M and Veraverbeke S 2021 Overwintering fires in boreal forests *Nature* **593** 399–404
Serreze M C, Barrett A P, Stroeve J C, Kindig D N and Holland M M 2009 The emergence of surface-based Arctic amplification *Cryosphere* **3** 11–19
Treharne R, Bjerke J W, Tømmervik H, Stendardi L and Phoenix G K 2019 Arctic browning: impacts of extreme climatic events on heathland ecosystem CO2 fluxes *Glob. Change Biol.* **25** 489–503
van Wijk M T *et al* 2003 Long-term ecosystem level experiments at Toolik Lake, Alaska, and at Abisko, Northern Sweden: generalizations and differences in ecosystem and plant type responses to global change *Glob. Change Biol.* **10** 105–23
Welp L R, Randerson J T and Liu H P 2007 The sensitivity of carbon fluxes to spring warming and summer drought depends on plant functional type in boreal forest ecosystems *Agric. For. Meteorol.* **147** 172–85
Wolf S *et al* 2016 Warm spring reduced carbon cycle impact of the 2012 US summer drought *PNAS* **113** 5880–5
Yi Y, Kimball J S, Watts J D, Natali S M, Zona D, Liu J, Ueyama M, Kobayashi H, Oechel W and Miller C E 2020 Investigating the sensitivity of soil heterotrophic respiration to recent snow cover changes in Alaska using a satellite-based permafrost carbon model *Biogeosciences* **17** 5861–82
Yin Y, Ciais P, Chevallier F, Li W, Bastos A, Piao S, Wang T and Liu H 2018 Changes in the response of the northern hemisphere carbon uptake to temperature over the last three decades *Geophys. Res. Lett.* **45** 4371–80
Yue C, Ciais P, Bastos A, Chevallier F, Yin Y, Rödenbeck C and Park T 2017 Vegetation greenness and land carbon-flux anomalies associated with climate variations: a focus on the year 2015 *Atmos. Chem. Phys.* **17** 13903–19
Zani D, Crowther T W, Mo L, Renner S S and Zohner C M 2020 Increased growing-season productivity drives earlier autumn leaf senescence in temperate trees *Science* **370** 1066–71
Zhang Y, Parazoo N C, Williams A P, Zhou S and Gentine P 2020 Large and projected strengthening moisture limitation on end-of-season photosynthesis *PNAS* **117** 9216–22
Zscheischler J *et al* 2014 A few extreme events dominate global interannual variability in gross primary production *Environ. Res. Lett.* **9** 035001